Electronic Supplementary Information

DCMiC: A Double Cylinder Micro-Chamber Platform for High-Throughput Drug Screening and Modeling of Microenvironmental Resistance in Ewing Sarcoma

Jaehun Lee[a,†], Muyi Ye[b,†], Mikayla Ybarra[a,c], Joy Fei[b], Yuan Gao[b,e]*, and Chao Ma[a,c,d,e]*

[a]Department of Cancer Sciences, Cleveland Clinic Research, Cleveland, OH 44195, USA

[b]Department of Pharmacology, Case Western Reserve University School of Medicine, Cleveland, OH 44106, USA

[c]Department of Pathology, Case Western Reserve University School of Medicine, Cleveland, OH 44106, USA

[d]Department of Molecular Medicine, Cleveland Clinic's Lerner College of Medicine of Case Western Reserve University School of Medicine, Cleveland, OH 44195, USA

[e]Case Comprehensive Cancer Center, Case Western Reserve University School of Medicine, Cleveland, OH 44106, USA

[†]These authors contribute equally.

*Correspondence should be addressed to Y. G. (yxg811@case.edu) or C. M. (mac7@ccf.org).

Abstract. This Supplementary Information includes all additional information as noted in the text.

Table of Contents

Figures

Tables

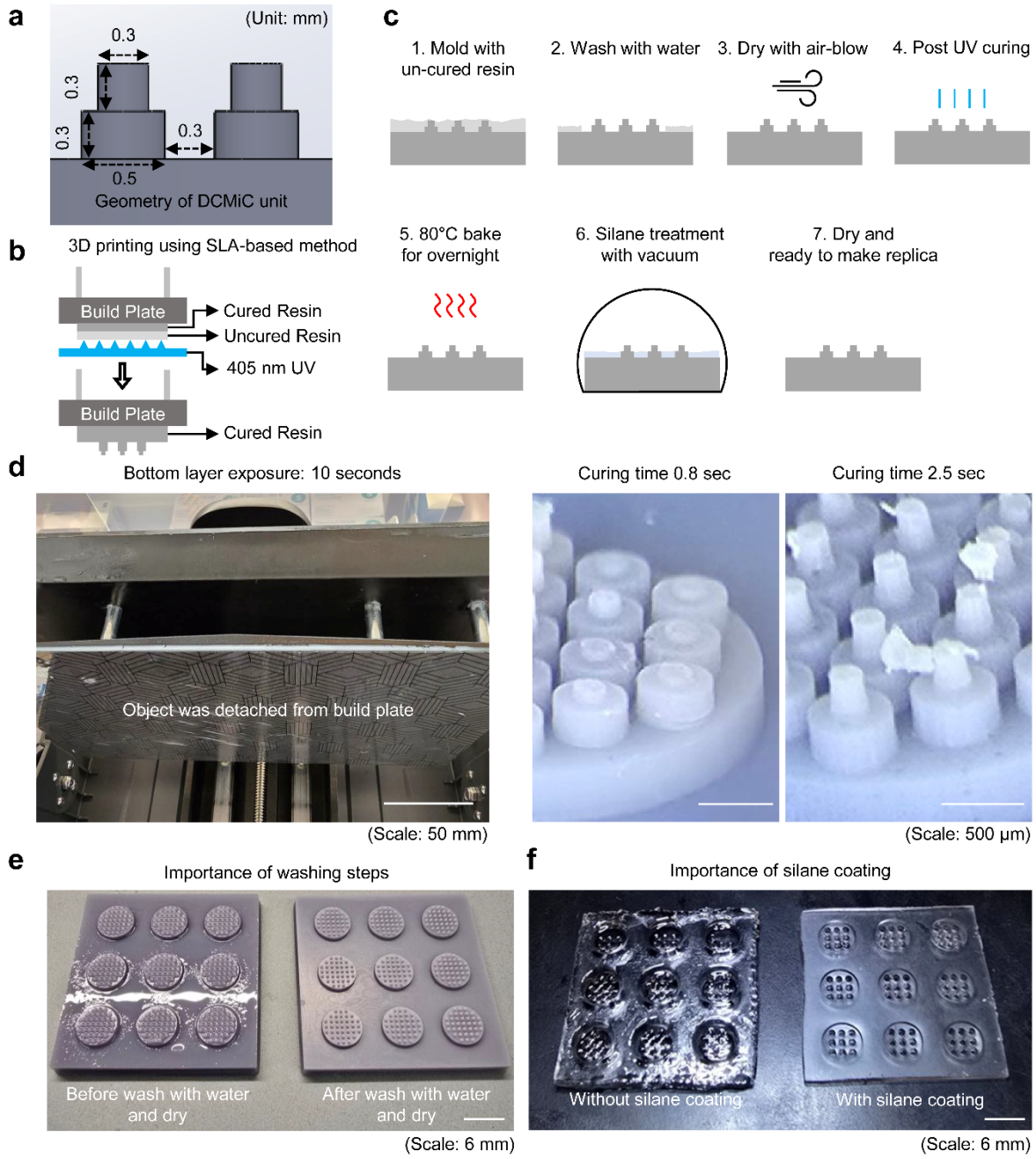

Figure S1. Overview of the SLA-Based 3D Printing Process and Key Troubleshooting Steps for Mold Fabrication. (**a**) Geometrical information of DCMiC master mold. (**b**) Schematic of fabrication mechanism. (**c**) Step-by-step schematic of the fabrication workflow using an SLA 3D printer, including resin curing, sequential washing, UV post-curing, baking, silane treatment, and final preparation for PDMS replication. (**d**) Effect of bottom layer (the initial resin layers directly attached to the build plate), UV exposure, and curing time on print quality. Left: While extending the bottom layer exposure time does not markedly affect structure formation, excessively long exposure significantly increases total printing time. Inadequate exposure (10 seconds) can cause detachment of the printed object from the build plate during fabrication. In this study, the bottom layer exposure time was set to 35 seconds. Middle: Short curing time (0.8 second) results in incomplete formation of microstructures. Right: Excessive curing time (2.5 seconds) leads to the formation of unintended residual structures surrounding the microfeatures. In this study, a curing time of 1.5 seconds was employed to ensure accurate and reproducible microstructure fabrication. Data were collected from three technical replicates (n = 3) with consistent outcomes. (**e**) Mold surfaces before and after thorough water washing and drying, showing that residual resin must be completely removed for a clean surface.[1] (**f**) PDMS replicas from molds without and with silane coating, demonstrating that silane treatment is essential for proper curing and clean demolding.

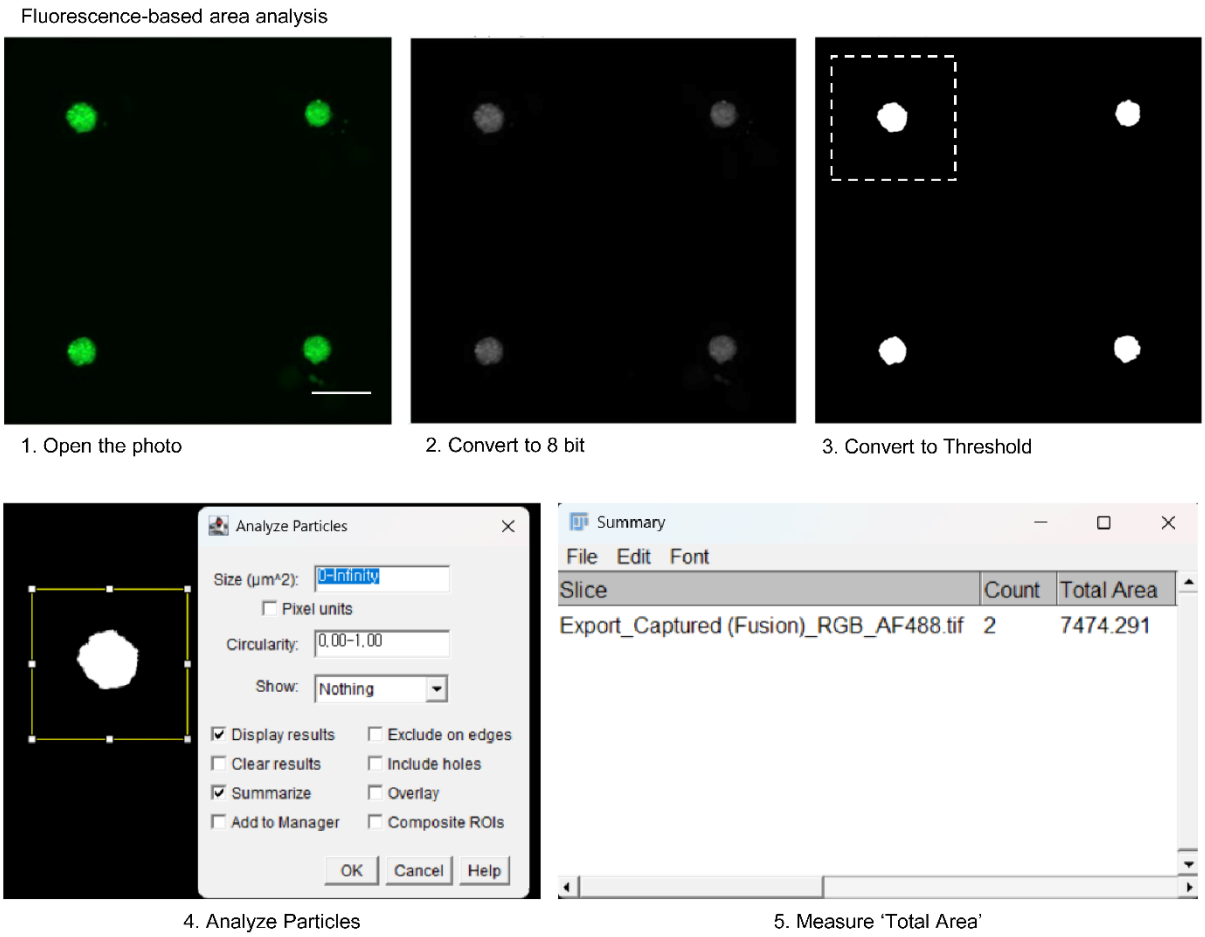

Figure S2. Spheroid Area and Viability Analysis Using ImageJ, with Representative Images and Workflow. (Scale bar: 200 µm)

0) Perform area-based analysis using the ImageJ software.

1) Open the image to be analyzed in ImageJ and set the appropriate scale.

*The scale may vary depending on the microscope used, so it is essential to confirm the pixel-to-scale ratio (e.g., µm/pixel) for the specific microscope settings.

2) Convert the image to 8-bit,

3) Then use the Threshold function to convert the image so that pixel areas can be quantified.

4) Select the area to be measured using the Selection Tool,

5) Then go to the Analyze tab and choose Analyze Particles to perform the measurement.

The remission analysis before and 48 hours after drug treatment was performed by quantifying the area of live cells. Live cells were identified based on GFP fluorescence. Since live and dead cells emit at 488 nm and 555 nm, respectively, fluorescence images were captured at both wavelengths. The live cell area and dead cell area were independently analyzed to calculate cell viability.

Table S1. SLA 3D Printing Conditions for Reliable DCMiC Fabrication.

Machine type	ELEGOO Saturn 4 Ultra
Mirror	LCD mirror
Resin type	Water Washable 2.0 Photopolymer Resin (Ceramic Grey), ELEGOO
Resin density	1.100 g/ml
Layer height	0.020 mm
Bottom layer count	5
Exposure time	1.5 second
Bottom exposure time	35 second
Transition layer count	20
Transition type	Linear

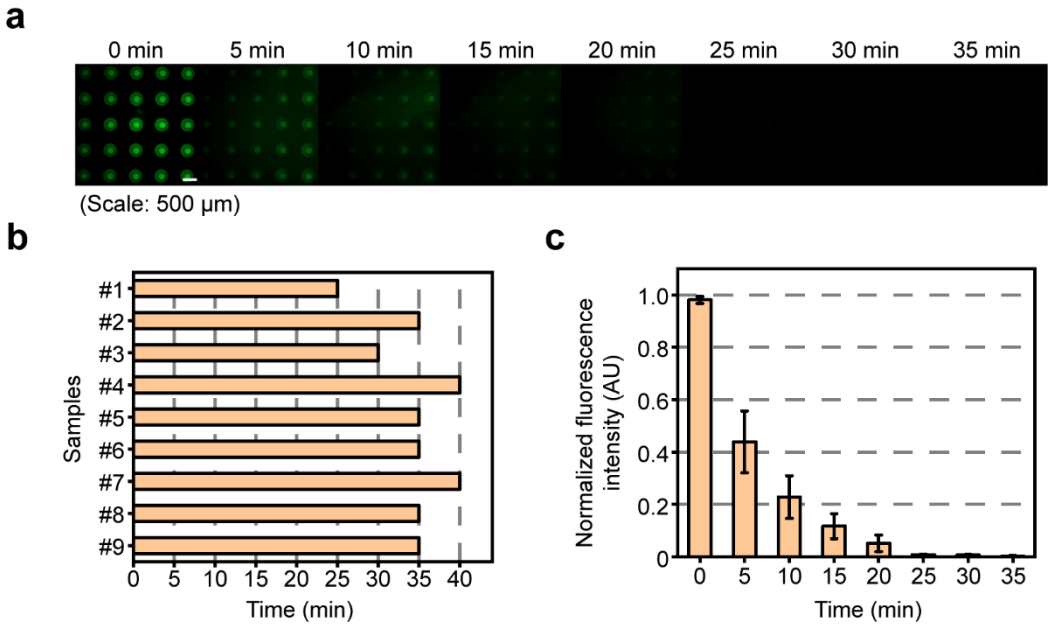

Figure S3. Assessment of Molecular Diffusion within the DCMiC. (**a**) Time-lapse fluorescence images showing the diffusion of fluorescein within the DCMiC from 0 to 35 min. The fluorescence intensity gradually decreased as the dye diffused into the surrounding medium. Scale bar: 500 μm. (**b**) Quantification of diffusion time across nine independent samples, demonstrating consistent diffusion kinetics among replicates. Data was collected from 9 independent wells. (**c**) Normalized fluorescence intensity over time shows a rapid decrease within the first 15 minutes and reaches equilibrium by 30–35 minutes, indicating efficient molecular diffusion within the DCMiC. Data was collected from 3 independent experiments (n=3) with total 225 DCMiC wells.

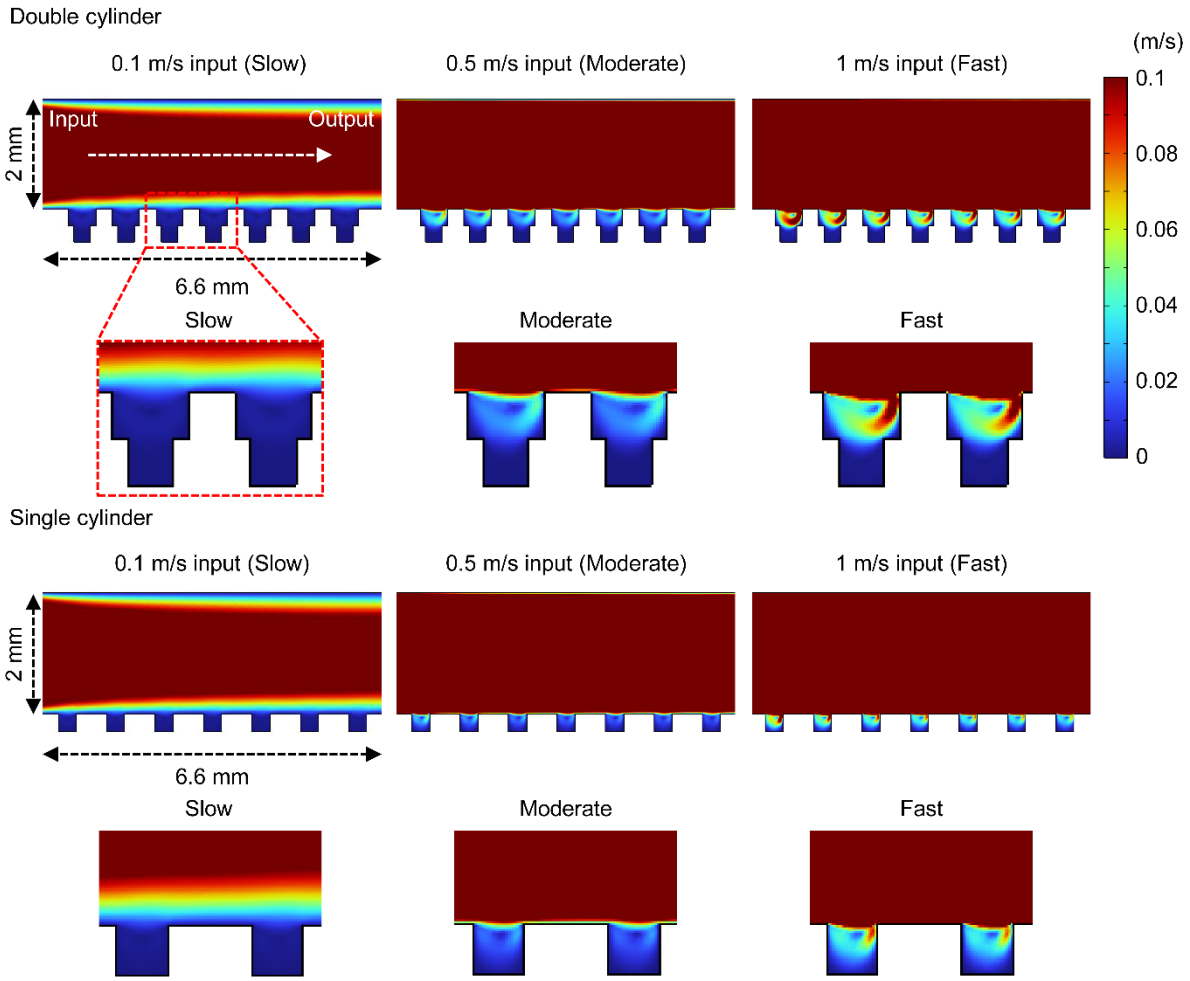

Figure S4. Estimation of Pipetting-Induced Flow and Computational Simulation. To quantify the hydrodynamic conditions generated by manual liquid handling, we estimated the exit velocities from a standard 200 µL pipette tip during dispensing into a 96-well plate. The inner diameter of a typical 200 µL pipette tip is approximately 0.8 mm, yielding a cross-sectional area (A) of 5.0 × 10^{-7} m^2. The volumetric flow rate (Q) and exit velocity (v) were determined using:

$$Q = \frac{V}{t} \quad v = \frac{Q}{A}$$

where V = 2.0 × $10^{-7}$$m^3$ (200µl) is the dispensed volume, t is the dispensing time. Based on typical laboratory practices, three dispensing speeds were analyzed: fast (0.4 s), moderate (0.8 s), and slow (4.0 s) for each 200 µL dispensed. The resulting exit velocities were 1.0 m/s, 0.5 m/s, and 0.1 m/s, respectively. To assess shear stress and velocity fields acting on cells, two-dimensional computational fluid dynamics (CFD) simulations were performed using COMSOL Multiphysics® v6.2 (COMSOL AB, Stockholm, Sweden). The computational domain was modeled as a rectangular fluid layer with a height of 2 mm, representing the medium layer above the cell culture surface in a single well. Three inlet velocities were examined: 0.1, 0.5, and 1.0 m/s, spanning the experimentally estimated pipetting velocities (0.1–1.0 m/s). All simulations assumed incompressible, laminar flow with no-slip boundary conditions at the bottom surface (cell layer) and an outlet pressure fixed at 0 Pa. The resulting velocity field maps were analyzed to quantify the hydrodynamic forces acting on cells during routine media exchange and reagent addition. Simulation analysis confirmed that spheroids could be stably maintained without inducing local flow disturbances under the range of conditions typically applied during routine handling in DCMiC platform. When the spheroid size exceeds the well depth, those in a single-cylinder structure are directly exposed to shear stress from the main flow, whereas the double-cylinder design effectively shields the spheroids from such direct exposure.

Table S2. Cost Comparison Between DCMiC and Commercially Available Platforms. Assumptions for the cost of calculation of DCMiC: 3D Printer: Elegoo Saturn ($400–$600, amortization excluded), Resin: Water Washable Resin, $35/L, Resin Use: 10 mL per mold, PDMS: Sylgard 184: $150/kg, PDMS Use: 20 g per mold, Mold Reuse: 5 times. With an initial setup consisting of an SLA printer (e.g., Elegoo Saturn 4, approximately $400–$600), standard resin ($35/L), and PDMS ($150/kg), the system allows for dozens to hundreds of reuses and offers flexibility for design modifications.[2-4] This comparison considers only material costs and retail prices,

Platform	Cost per Unit (USD)	Reusability	Estimated Cost per Use (USD)	Notes
DCMiC (Elegoo + PDMS)	$3.35	Yes (At least 5 uses)	$0.67	Based on $35/L resin (10 mL/mold) and $150/kg PDMS (20 g/mold)
ULA Plate (e.g., Corning 7007)	$13.50	No	$13.50	Standard 96-well U-bottom format
Corning Spheroid Plate (CLS4520)	$32.50	No	$32.50	Features ultra-low attachment coating
AggreWell™ 400 (STEMCELL)	$100.00	No	$100.00	High-throughput microwell format

excluding indirect, research and development, and ancillary expenses.

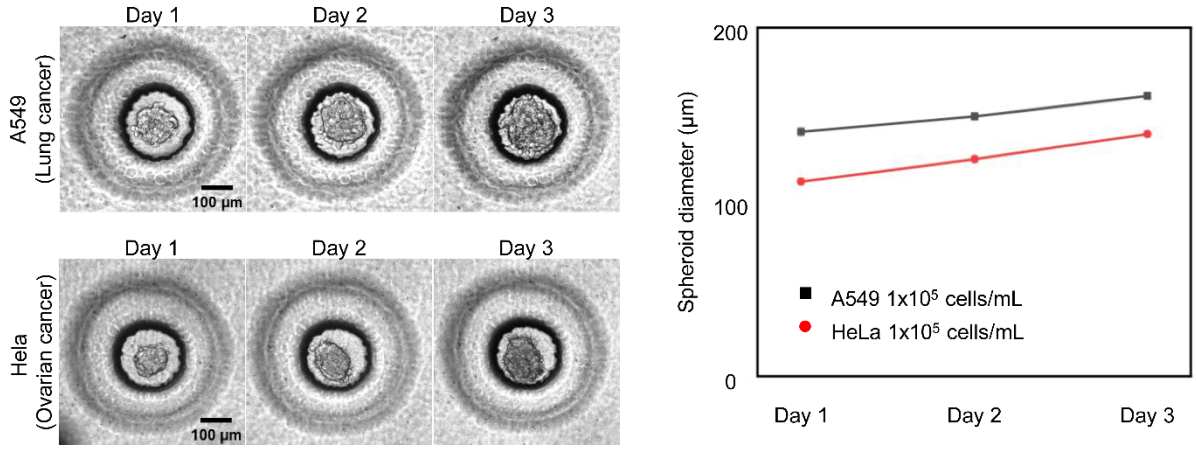

Figure S5. Spheroid Formation with A549 and HeLa as Validation of the DCMiC's Versatility. Bright-field images and growth curves demonstrate spheroid formation of A549 (human lung cancer) and HeLa (human cervical cancer) cells at a seeding density of 1×10^5 cells/mL over a 3-day culture period. Both cell types successfully formed uniform spheroids that exhibited progressive growth in diameter from Day 1 to Day 3. Quantitative analysis shows a steady increase in spheroid size, with A549 spheroids reaching ~180 µm and HeLa spheroids ~150 µm in diameter by Day 3, confirming that the DCMiC platform supports reproducible spheroid formation beyond Ewing sarcoma cell lines. Scale bars: 100 µm.

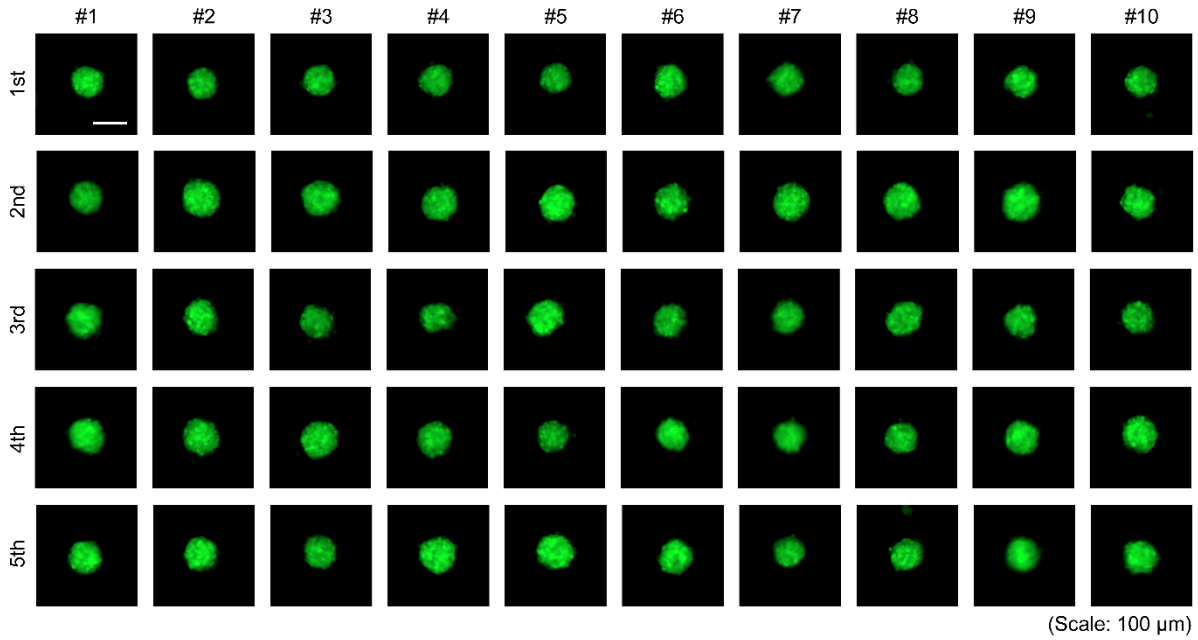

Figure S6. Representative Fluorescent Images of Spheroids Generated in the Same DCMiC Wells over Five Consecutive Cycles of Use. The consistent size and morphology across all cycles demonstrate that the DCMiC platform can repeatedly produce uniform spheroids even after multiple uses.

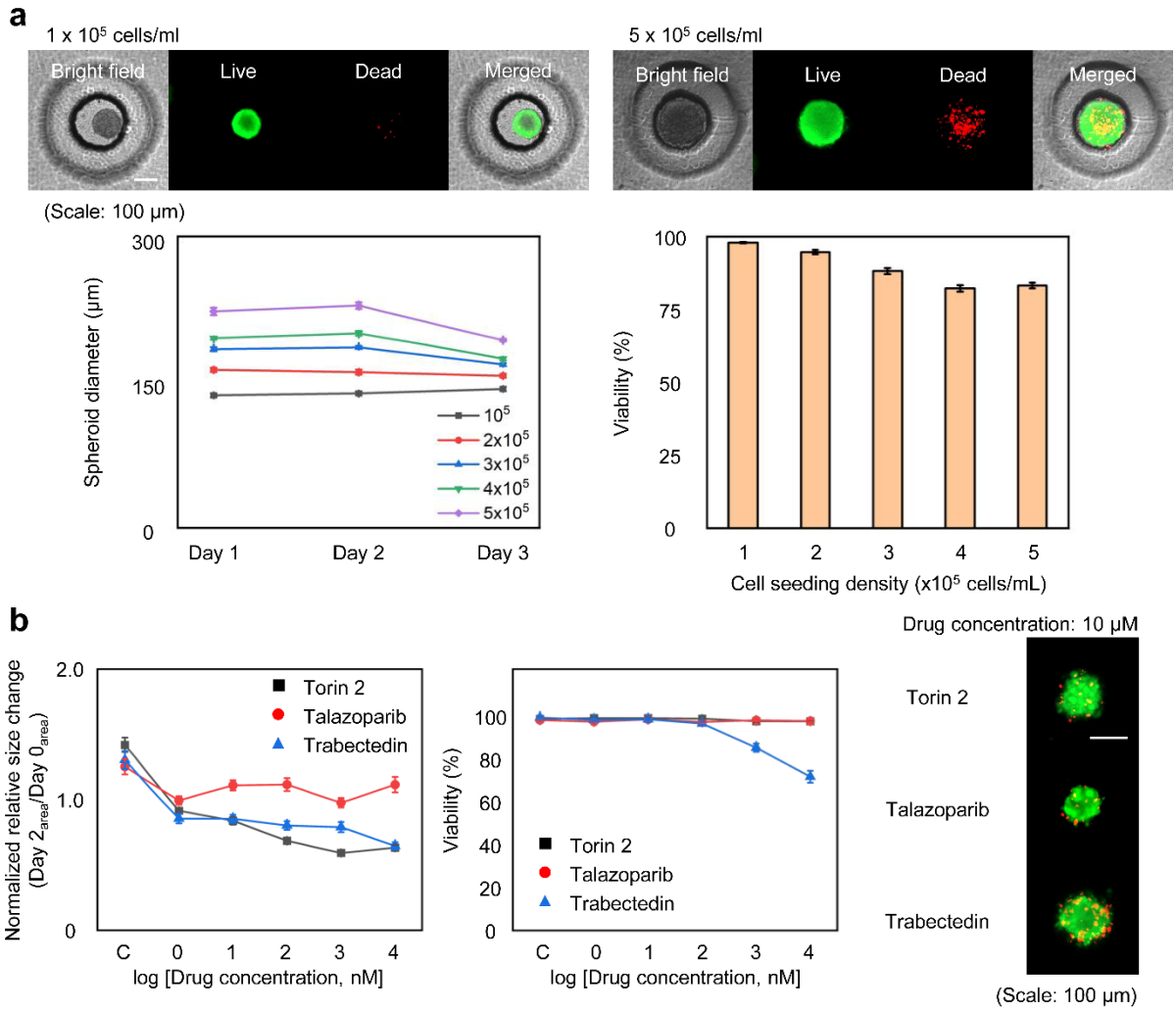

Figure S7. Optimization of Fibroblast Spheroid Formation and Assessment of Remission and Viability in Response to Torin 2, Talazoparib, and Trabectedin. (**a**) Spheroid diameter (left) and cell viability (right) of Normal Human Lung Fibroblast (NHLF) spheroids were assessed across different seeding densities (1×10^5 to 5×10^5 cells/mL) over a 3-day culture period. At a seeding density of 1×10^5 cells/mL, spheroid diameter began to increase from Day 1, whereas spheroids generated at higher densities exhibited progressive reductions in size over time, suggesting excessive compaction. Viability was also highest at 1×10^5 cells/mL (>95%) and progressively decreased at higher densities. This density was therefore selected as the standard condition for subsequent experiments to match the seeding density used in sarcoma spheroid cultures and ensure optimal growth and survival. Data was collected from 3 independent experiments (n=3) with 45 total images analyzed. (**b**) Viability and spheroid remission were assessed in NHLF monoculture spheroids treated with the indicated drugs to confirm that stromal fibroblasts do not contribute to nonspecific viability loss in subsequent sarcoma–fibroblast heterotypic spheroid assays, and the drug concentrations used in the heterotypic spheroid testing fall within ranges that exert minimal effects on fibroblasts. Data was collected from 3 independent experiments (n=3) with 45 total images analyzed.

Table S3. Detailed statistical results for Figures 4c.

Comparison	t	df	Mean of difference	95% CI	P-value
A673 (Torin 2) Mono vs Hetero	12.28	88	–18.18	–21.13 ~ –15.24	<0.0001
A673 (Talazoparib) Mono vs Hetero	7.31	88	–10.56	–13.43 ~ –7.69	<0.0001
A673 (Trabectedin) Mono vs Hetero	12.47	88	–19.52	–22.63 ~ –16.41	<0.0001
TC-71 (Torin 2) Mono vs Hetero	16.69	88	–25.20	–28.20 ~ –22.20	<0.0001
TC-71 (Talazoparib) Mono vs Hetero	15.66	88	–22.33	–25.17 ~ –19.50	<0.0001
TC-71 (Trabectedin) Mono vs Hetero	12.17	88	–21.76	–25.31 ~ –18.20	<0.0001
RH-1 (Torin 2) Mono vs Hetero	7.99	88	–20.71	–25.86 ~ –15.56	<0.0001
RH-1 (Talazoparib) Mono vs Hetero	8.76	88	–18.95	–23.24 ~ –14.66	<0.0001
RH-1 (Trabectedin) Mono vs Hetero	5.84	88	–13.01	–17.43 ~ –8.59	<0.0001

Table S4. Detailed statistical results for Figures 6(b, c).

Comparison	t	df	Mean of difference	95% CI	P-value
A673 (Torin 2) Control vs TGF-β	5.00	88	–11.67	–16.31 ~ –7.03	<0.0001
A673 (Talazoparib) Control vs TGF-β	3.89	88	– 7.35	–11.10 ~ –3.59	0.0002
A673 (Trabectedin) Control vs TGF-β	4.42	88	– 8.63	–12.51 ~ –4.75	<0.0001
TC-71 (Torin 2) Control vs TGF-β	3.19	88	–6.38	–10.34 ~ –2.40	0.002
TC-71 (Talazoparib) Control vs TGF-β	4.86	88	–9.09	–12.81 ~ –5.38	<0.0001
TC-71 (Trabectedin) Control vs TGF-β	6.14	88	–13.62	–18.03 ~ –9.21	<0.0001
RH-1 (Torin 2) Control vs TGF-β	6.60	88	–14.05	–18.28 ~ –9.82	<0.0001
RH-1 (Talazoparib) Control vs TGF-β	5.33	88	–9.53	–13.09 ~ –5.98	<0.0001
RH-1 (Trabectedin) Control vs TGF-β	4.46	88	–10.65	–15.39 ~ –5.91	<0.0001
A673 (Torin 2) Heterotypic Without vs With inhibitor	5.44	88	12.19	7.73 ~ 16.64	<0.0001
A673 (Talazoparib) Heterotypic Without vs With inhibitor	5.88	88	9.18	6.08 ~ 12.28	<0.0001
A673 (Trabectedin) Heterotypic Without vs With inhibitor	5.87	88	11.99	7.93 ~ 16.05	<0.0001
TC-71 (Torin 2) Heterotypic Without vs With inhibitor	5.01	88	9.45	5.71 ~ 13.2	<0.0001
TC-71 (Talazoparib) Heterotypic	7.23	88	10.85	7.87 ~ 13.83	<0.0001

Without vs With inhibitor					
TC-71 (Trabectedin)					
Heterotypic Without vs With inhibitor	8.23	88	15.85	12.02 ~ 19.67	<0.0001
RH-1 (Torin 2)					
Heterotypic Without vs With inhibitor	4.59	88	8.45	4.79 ~ 12.11	<0.0001
RH-1 (Talazoparib)					
Heterotypic Without vs With inhibitor	4.09	88	9.54	4.91 ~ 14.17	<0.0001
RH-1 (Trabectedin)					
Heterotypic Without vs With inhibitor	5.52	88	14.91	9.54 ~ 20.28	<0.0001

References

1. C. Con and B. Cui, *Nanoscale Res Lett*, 2013, **8**, 394.
2. T. D. Ngo, A. Kashani, G. Imbalzano, K. T. Nguyen and D. Hui, *Composites Part B: Engineering*, 2018, **143**, 172-196.
3. M. J. Lerman, J. Lembong, G. Gillen and J. P. Fisher, *Appl Phys Rev*, 2018, **5**, 041109.
4. E. Steinberg, R. Friedman, Y. Goldstein, N. Friedman, O. Beharier, J. A. Demma, G. Zamir, A. Hubert and O. Benny, *Communications Biology*, 2023, **6**, 1157.